Contrib Mineral Petrol (1996) 125: 359–374

Lucy M. Thompson · John G. Spray

Pseudotachylyte petrogenesis: constraints from the Sudbury impact structure

Received: 15 March 1996 / Accepted: 15 June 1996

Abstract Pseudotachylytes and their host rocks from the North Range of the 1.85 Ga Sudbury impact structure have been investigated using analytical scanning electron microscopy, electron microprobe analysis and XRF spectrometry. The results show that the pseudotachylytes were produced in high-speed slip zones by the frictional comminution and selective melting of wall rock lithologies. The preferential assimilation of hydrous ferromagnesian phases during frictional melting produced relatively basic melts, leaving the more mechanically resistant quartz and, to a lesser extent, plagioclase as included mineral clasts. Three distinct assemblages are identified within the pseudotachylytes: (a) pre-impact (>1.85 Ga) rock and mineral clasts derived from host lithologies; (b) a syn- to immediately post-impact (1.85 Ga), rapidly cooled, quartz + sanidine + labradorite + phlogopitic biotite matrix assemblage, formed due to crystallization from a melt at 800–900°C and (c) a post-impact (<1.85 Ga) retrograde assemblage which overprints both clasts and matrices. Field evidence indicates that most pseudotachylyte formed in large-displacement fault systems during gravitational collapse of the impact-generated transient cavity. The Sudbury pseudotachylytes, like endogenic pseudotachylytes, were generated by frictional melting on fault surfaces. The difference is primarily one of scale. Large (km) displacements occurring on impact-induced ring faults can generate immense volumes of friction melt resulting in spectacular pseudotachylyte bodies up to 0.5 km thick and more than 10 km long.

Introduction

Pseudotachylyte is one of the few magmatic rocks to originate by purely dynamic means under conditions of high and ultrahigh rates of strain (Philpotts 1964; Maddock 1983; Spray 1993). Most pseudotachylytes are found in close association with fracture or slip systems. They are considered the only rock type diagnostic of seismogenic activity (Sibson 1975). Accounts of pseudotachylytes from endogenic faults are now commonplace, with much of that work focusing on their structural setting. In contrast, comparatively few detailed investigations have been made of the chemistry, mineralogy and petrology of pseudotachylytes, especially those associated with the type setting for pseudotachylyte generation: impact structures.

The term pseudotachylyte was created by Shand (1916) following his work on the Vredefort Dome of South Africa; a structure that is now widely held to be one of Earth's largest impact basins (Martini 1991; Therriault et al. 1993). Unlike endogenically generated examples, which are typically <10 cm thick, pseudotachylyte developed in the larger (>100 km diameter) impact structures can reach tens and even hundreds of metres in thickness to form substantial pod- or dyke-like bodies.

Pseudotachylyte typically possesses a black, glassy or, more commonly, a fine- to medium-grained groundmass (matrix), similar in appearance to tachylytes (glassy basaltic rocks) after which they were named. The matrix encloses clasts of mineral and rock fragments, mainly derived from the immediate wall rocks. Microigneous textures, spherulites, flow-banding and chilled margins, along with the presence of vesicles, amygdales, sulphide "droplets" and embayed (partly digested) wall rock mineral fragments, all indicate pseudotachylyte formation via melting, and not solely by cataclasis (Magloughlin and Spray 1992). However, cataclastic margins and clasts of cataclastic material occur within many pseudotachylytes, indicating that the early stages of their formation involves comminution. This is supported by experimental work (Spray 1987, 1988, 1995) and investigations of drill bit-rock interactions (Killick 1990; Kennedy and Spray 1992), the results of which have revealed the intrinsic spatial and temporal connections be-

L. M. Thompson · J. G. Spray (✉)
Department of Geology, University of New Brunswick,
Bailey Drive, Fredericton, New Brunswick, E3B 5A3, Canada

Editorial responsibility: J. Hoefs

tween comminution and frictional melting at high strain rates.

This work deals with the petrogenesis of pseudotachylyte in another of Earth's larger impacts: the Sudbury multi-ring structure of Ontario, Canada.

Regional geological setting and origin of the Sudbury structure

The Sudbury structure was formed at 1.85 Ga (Krogh et al. 1984) due to hypervelocity meteorite impact into Archean and Proterozoic lithologies of the Canadian Shield (Fig. 1). The structure comprises a shocked, fractured and faulted basement underlying a 60×30 km, 2.5 km thick, layered impact melt sheet, the Sudbury igneous complex (SIC), which is overlain by fallback breccia, the Onaping Formation (Peredery 1972; Stöffler et al. 1994). This passes up into mudstones and turbiditic sandstones which, together with the Onaping Formation, constitute the so-called Whitewater group (Rousell 1984). Hybrid models have also been invoked for the origin of the Sudbury structure, whereby the magmatic activity that generated the SIC has been attributed to lower crust-mantle disturbance and melting in response to impact (Naldrett 1984). However, Sr and Nd isotopic data indicate an exclusively crustal origin for the SIC, requiring no mantle-derived component (Faggart et al. 1985; Deutsch 1994).

It was the discovery of shatter cones, developed in basement rocks up to ~20 km from the SIC, that led Dietz (1964) to suggest an origin by meteorite impact. Support for an impact origin also comes from the presence of planar deformation features (PDFs), including Brazil twin lamellae, in minerals from the basement, and from basement clasts incorporated into the pseudotachylytes and the Onaping Formation (French 1968; Joreau et al. 1996). In quartz, PDFs occur with up to three sets of lamellae, considered diagnostic of shock pressures ≥10 GPa (Hörz 1968) and of at least Shock Stage 1 (Müller-Mohr 1992; Stöffler and Langenhorst 1994). PDFs have also been observed in Sudbury plagioclase (Dressler 1984), and Speers (1957, p 502) described optically isotropic plagioclase in clasts within pseudo-

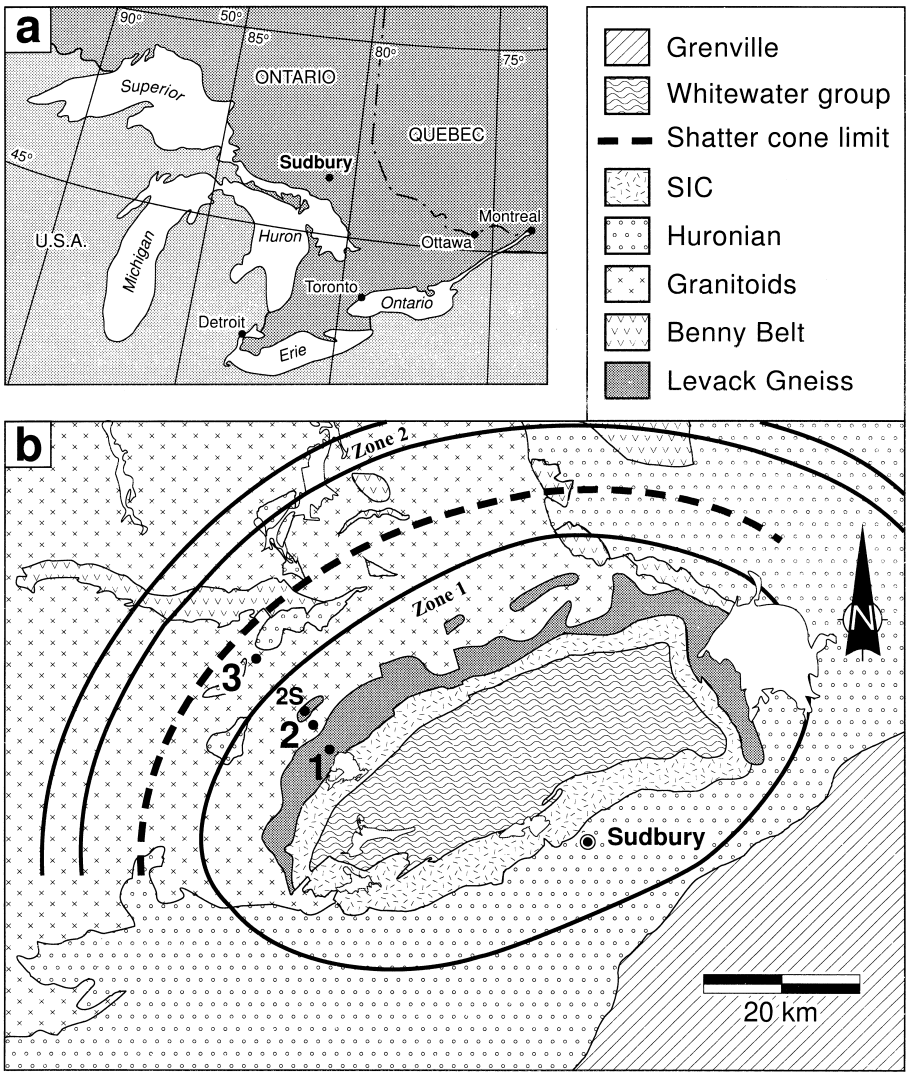

Fig. 1 **a** Location of Sudbury relative to the Canada/U.S.A. Great Lakes region. **b** Geological setting of the Sudbury structure showing site locations 1–3. (*SIC* Sudbury igneous complex). Pseudotachylyte-rich zones occur around the SIC (*Zone 1*) and 25–35 km beyond the SIC (*Zone 2*) on this map. Shatter cone limit after Dietz (1964)

tachylytes from north and east of the SIC which is probably diaplectic glass (formation pressure >26 GPa, Ostertag 1983).

The present elliptical shape of the SIC and overlying rocks (Fig. 1b) is attributed to post-impact tectonic deformation due to northwest-directed shortening during the mid-Proterozoic (~1.9–1.7 Ga) Penokean orogeny (Hurst and Farhat 1977; Shanks and Schwerdtner 1991). The southeastern part of the structure was overprinted by the late Proterozoic (~1.0 Ga) Grenvillian orogeny (Jamieson et al. 1992). The Sudbury region is pervaded by a number of basic dyke swarms. Those that predate the impact include the 2.45 Ga Matachewan dykes (Heaman 1988) and the 2.2 Ga Nipissing Diabases (Corfu and Andrews 1986).

A distinctive feature of the Sudbury structure and the focus of this work is the pseudotachylyte that pervades the area. It has been previously referred to as Levack Breccia in the North Range (north of the SIC) and Frood Breccia in the South Range (south of the SIC) and, regionally, as Sudbury Breccia (Yates 1938; Fairbairn and Robson 1942; Speers 1957; Zurbrigg 1957; Müller-Mohr 1992). Based on the distribution of pseudotachylyte and on other constraints, it is likely that the original diameter of the Sudbury structure was at least 200 km and probably as much as 250 km (Lakomy 1990; Grieve et al. 1991; Thompson and Spray 1994; Spray and Thompson 1995; Deutsch et al. 1995).

The Sudbury pseudotachylytes

The pseudotachylytes range in size from <1 mm thick veinlets to large dyke-like bodies several hundred metres in thickness. Pseudotachylyte abundance decreases radially away from the SIC. At least four discontinuous, subconcentric zones of more intense pseudotachylyte development occur at 0–13 km, 25–35 km, 42–48 km and 78–80 km north of the SIC within the North Range (Thompson and Spray 1994; Spray and Thompson 1995). Comparable distributions have also been documented by Dressler (1984), Peredery and Morrison (1984) and Müller-Mohr (1992).

The innermost zone forms a halo to the SIC in which pseudotachylyte is pervasive on all scales (Fig. 1b, Zone 1). Here, thin veinlets are ubiquitous and the spectacular larger dyke-like bodies are common (e.g. Fig. 2a). The largest known single occurrence at Sudbury, and in the world, is the Frood-Stobie pseudotachylyte of the South Range which is up to 0.5 km wide and >11 km in length. This is host to the largest Ni-Cu deposit in the Sudbury mining camp. The maximum size and frequency of occurrence of pseudotachylyte decreases in each successive concentric zone northwards from the SIC. Relatively minor volumes are developed in the intervening areas, some of which equate with the "quiet zones" of Dressler (1984, p 124). Any concentric structure developed south of the SIC within the South Range, with the exception of the innermost zone (Zone 1, Fig. 1b), has been largely obscured by post-impact tectonometamorphism.

The majority of the Sudbury pseudotachylytes possess dark matrices enclosing subangular to rounded clasts of the immediate wall rock (Fig. 2b). Matrices tend to weather greenish grey, with fresh surfaces revealing a hard, flinty rock exhibiting sub-conchoidal fracture. The clasts range from millimetre-size fragments through to blocks hundreds of metres across. Clasts make up ~40–60% of the pseudotachylytes, but less than this where injected into fractures. The pseudotachylyte is commonly associated with lithological contacts (e.g. between basic dykes and gneisses; Fig. 2c). Pseudotachylyte injections have sharp contacts with their wall rocks (Fig. 2d). Pseudotachylytes remaining on their generating surfaces have sharp to diffuse contacts. Diffuse contacts appear mesoscopically ductile, but are cataclastic at the microscopic scale (Thompson and Spray 1994). Less commonly, red, light grey and flow-foliated matrices occur. Within the flow-foliated pseudotachylytes, the clasts are typically elongate and streaked out parallel to the flow layers of the matrix. The more peripheral pseudotachylytes of the Sudbury structure (>50 km beyond the SIC) grade into cataclastic rocks and true breccias.

Certain thin (<1 mm thick) pseudotachylytes occur as arcuate, overlapping veins which appear to define shatter cone surfaces, as have been observed at Vredefort (Martini 1991). Many of these pseudotachylytes form anastomosing networks similar to Lambert's (1981) so-called *Type A* veins. They are prevalent in the innermost zone (Zone 1, Fig. 1b) and may directly be shock generated. In contrast, the larger pseudotachylyte bodies tend to be associated with distinct planar surfaces, suggestive of generation planes similar to endogenic pseudotachylytes. These equate with Lambert's (1981) *Type B* variant. The thinner veins generally predate the larger dyke-like bodies, indicating that the former may have been generated during the passage and relaxation of the shock wave, and the latter during subsequent gravitational modification of the Sudbury structure. This work focuses on the *Type B* variety.

Sample locations and descriptions

Three main sites were chosen for detailed study, located 2.5, 5.5 and 18 km north of the outer rim of the SIC (Fig. 1b). Samples were obtained primarily by coring using a rock drill. The cores are 2.5 cm in diameter and up to 15 cm long. Several pairs of cores were taken from host rocks and adjacent pseudotachylytes at each site. Where possible, these were sampled within 10 cm of each other.

Site 1

Site 1 is a 40 m wide pseudotachylyte-rich zone within the Levack gneiss complex (Figs. 1b, 3a). It is located 2.5 km from the SIC, probably within its thermal aureole (Card 1994). The pseudotachylyte occurs as 0.1 to 2 m wide, matrix-rich zones enclos-

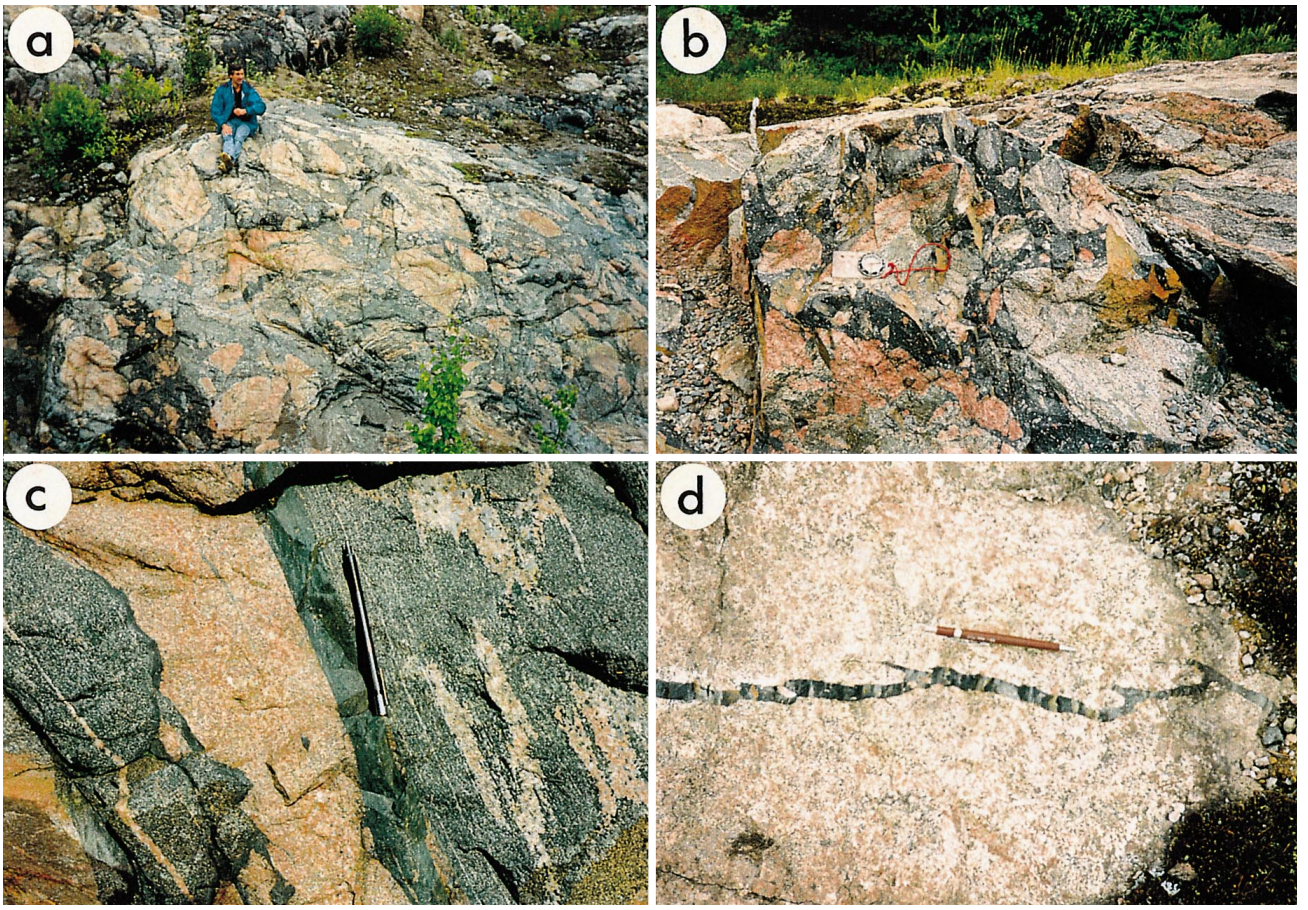

Fig. 2 **a** Large pseudotachylyte body at McCreedy West (0.5 km north of SIC). Note large, angular to subangular Levack felsic gneiss blocks set within darker matrix. **b** 2 m wide pseudotachylyte body with Levack gneiss inclusions (2.5 km north of SIC at Site 1). **c** 2 cm wide pseudotachylyte occurring between felsic and basic gneiss (immediately left of pen). Note the limited number of clasts and the sharp contacts with the host rocks (4 km north of the SIC). **d** Pseudotachylyte injection vein within felsic gneiss. Note sharp contacts and scarcity of clasts (2 km north of the SIC)

ing blocks of felsic and intermediate gneisses. The blocks are rounded, but the orientation of their foliations is coherent across the outcrop, demonstrating that block displacement and rotation were negligible. Two basic dykes are present, both of which show evidence of brecciation, indicating that they predate the Sudbury event (i.e. they are Matachewan or Nipissing bodies).

Site 2

Site 2 is located 5.5 km from the SIC, between the northern edge of the main Levack gneiss occurrence and a Levack inlier (Figs. 1b, 3b). This location is outside the thermal aureole of the SIC. The host rocks comprise Cartier granitoids with subordinate gneisses. Pseudotachylyte penetrates the granitoids and gneisses for up to 10 m north of the road where it connects to a 0.5 m thick body formed along a curviplanar face exposed in a road cutting. The granitoids are also cut by a small basic dyke which, on the south side of the road, exhibits a well-defined 5 cm thick pseudotachylyte vein along one contact. On the north side of the road, pseudotachylyte occurs along both contacts and within the dyke, carrying with it inclusions of both dyke and granitic material (Fig. 3b).

A subsidiary outcrop (Site 2S; Fig. 1b) was investigated 7.5 km from the SIC. Here the host rocks are migmatites of the Levack gneiss complex forming an inlier within Cartier granitoids. The pseudotachylyte occurs as an 11 m wide zone along a contact between migmatitic gneisses and a gabbroic dyke. The main body of pseudotachylyte occurs within the migmatite adjacent to the dyke.

Site 3

Site 3 is located 18 km from the SIC within the Cartier granitoids (Figs. 1b, 3c). It is situated at the southern edge of a shear zone that defines the southern boundary of the Archean Benny Belt (Card and Innes 1981). The sampled pseudotachylytes occur in a 30 m wide less-deformed zone. They exhibit dark, fine-grained matrices enclosing subrounded to rounded blocks of Cartier granitoid. At the northern end of the outcrop a megablock of Nipissing Diabase occurs within pseudotachylyte (Fig. 3c).

Analytical procedures

Twelve host rocks and three pseudotachylytes, including clasts, were analysed by X-ray fluorescence (XRF) spectrometry using a Philips PW 1410 spectrometer at UNB. Major element analysis was performed on glass disks prepared according to the method of Norrish and Hutton (1969). Disks were analysed at 40 mA and 40 kV. Raw data were reduced using linear regression calibration curves prepared using twenty international standards (Abbey 1983).

The pseudotachylytes and their host rocks were investigated using a JEOL 6400 digital scanning electron microscope equipped

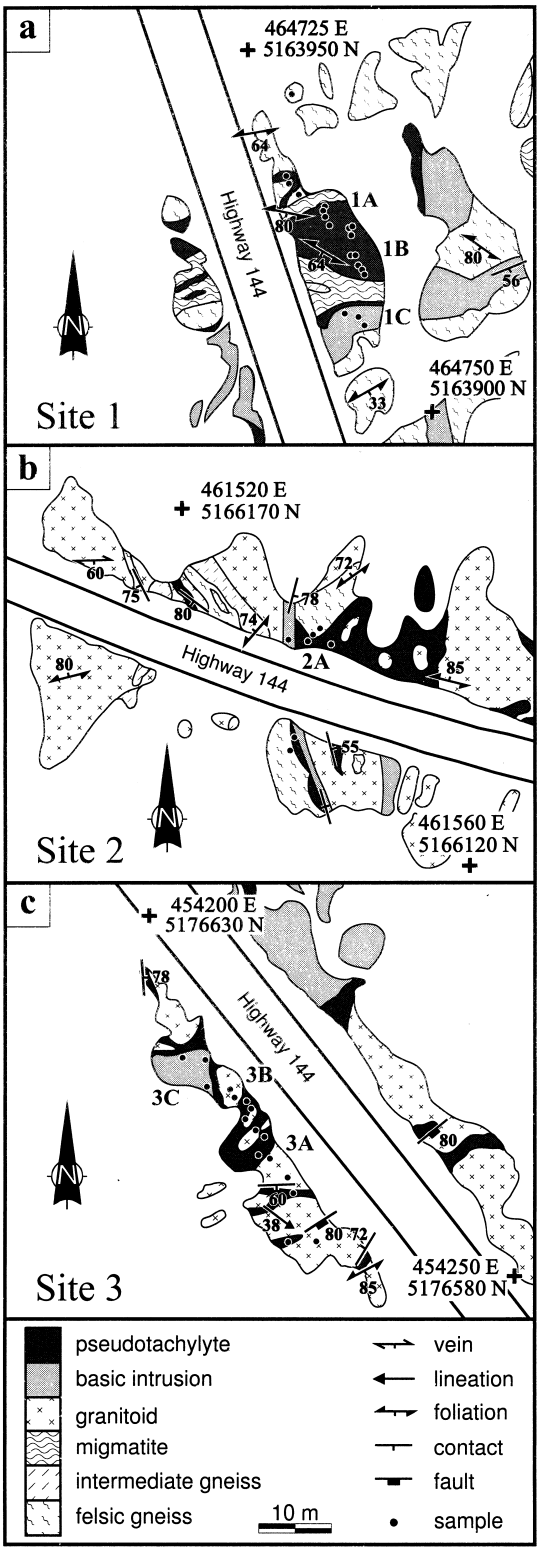

Fig. 3a–c Simplified geology of Sites 1, 2 and 3 showing pseudotachylyte-host rock relations and sampling (coring) points

with a Link Analytical eXL energy dispersive spectrometer (EDS) fitted with a Si(Li) LZ-4 Pentafet detector. All pseudotachylyte matrix analyses were determined in EDS mode at count times of 100 s, beam operating conditions of 15 kV and 2.5 nA and a working distance of 39 mm. Analyses were calibrated using a multi-element standards block (type 202–52) produced by the C.M. Taylor Corporation of Sunnyvale, California. The SEM backscattered electron (BSE) imagery was used to investigate the microtextures and mineralogy of the pseudotachylytes, accompanied by single spot analysis of individual minerals. Mineral analyses were also obtained from selected host rocks. Photomicrographs were obtained from BSE images using the same operating conditions as above, but at a reduced working distance (<19 mm).

Pseudotachylyte matrices were each rastered in 40 separate areas of ~2000 μm^2. Rastered areas were selected using the lowest viable magnification to avoid rock and mineral clasts. Raster analyses were also obtained for 30 matrix-plus-clast areas of ~100,000 μm^2 for each sample (i.e. bulk pseudotachylyte analyses). Energy dispersive was used instead of wavelength dispersive spectrometry (WDS) because not only does it enable rapid, simultaneous major element analysis, it can also operate at lower beam currents than WDS. This minimizes thermal excitation effects and, hence, alkali metal migration (e.g. Spray and Rae 1995).

Where alkali mobility was not deemed problematic, certain host rock minerals were analysed using a JEOL 733 electron microprobe equipped with four wavelength dispersive spectrometers (operating conditions: 15 kV and 10 nA at a working distance of 12 mm).

Chemistry

Limited data exist on the chemistry of pseudotachylytes. This is due primarily to the rock's composite nature. In order to understand how pseudotachylytes form, matrix compositions must be determined independently of included mineral and rock clasts. Analyses have been obtained following attempted physical separation of clasts from matrices (e.g. Sibson 1975; Dressler 1984). However, it is difficult to achieve complete separation because matrix phases and clasts can be of similar mineralogies and grain sizes. Hence, they may be indistinguishable. The microcrystalline nature typical of pseudotachylyte matrices and the microscopic size of some mineral clasts also make hand-picking untenable. Analyses of pseudotachylyte matrices have previously been obtained *in situ* using the electron microprobe in WDS mode with a defocused beam (e.g. Schwarzman et al. 1983; Reimold 1991; Killick 1994). Analytical scanning electron microscopy (ASEM) has also been used successfully on pseudotachylytes using rastered or defocused beams in EDS mode (Spray 1993) and this technique, along with XRF analysis, is the procedure used here.

Results from XRF bulk rock analysis and ASEM raster analysis of the Sudbury pseudotachylytes and their respective host rocks are given in Table 1. Both the bulk (P-b samples) and matrix-only (P-m samples) pseudotachylyte compositions span the intermediate field (52–66 wt% SiO_2), in contrast to the gneisses and granitoids (IG and F samples: >60 wt% SiO_2) and basic host rocks (B samples: ≤52 wt% SiO_2). These three main groups are shaded separately in Figs. 4 and 5.

The pseudotachylytes are more FeO-rich than the felsic gneisses and granitoids, but their FeO contents overlap with those of the intermediate gneisses and basic host

Table 1 Major element analyses of pseudotachylytes and host rocks. Site numbers correspond to those shown in Figure 3. Concentrations are in weight%. [*F* felsic gneiss/granitoid host rock, *P* pseudotachylyte, *IG* intermediate gneiss host rock, *B* basic intrusive host rock, *NA* not analysed, * total iron as FeO, *i* pseudotachylyte injection, *x* analysed by XRF, *r* analysed by raster scanning using ASEM, *b* bulk (matrix-plus-clasts) analysis, *m* matrix-only analysis, *LOI* loss on ignition]

Site 1

	F-1A/x	P-1A/bx	P-1A/br	P-1A/mr	F-1B/x	δ P-1B/br	γ P-1B/mr	β P-1B/ibr	α P-1B/imr	IG-1B/x	B-1C/x
SiO_2	61.67	59.40	62.99	56.80	69.28	63.77	53.75	52.98	50.52	60.84	52.29
TiO_2	0.93	0.69	0.76	0.96	0.35	0.72	1.22	0.40	0.26	0.93	1.57
Al_2O_3	16.02	14.90	14.97	16.47	14.51	17.01	17.78	13.62	11.06	16.10	12.54
FeO*	4.34	5.79	6.20	7.96	1.67	5.71	9.53	12.66	14.13	6.52	14.79
MnO	0.08	0.08	0.02	0.05	0.04	0.02	0.04	0.22	0.26	0.10	0.24
MgO	3.06	4.49	3.70	5.23	1.74	3.03	5.20	8.59	11.18	4.18	4.63
CaO	3.30	3.93	3.68	3.88	3.02	2.88	2.37	5.76	7.41	2.85	7.73
Na_2O	4.40	3.34	2.61	4.14	4.65	4.96	4.37	2.54	1.64	3.60	2.00
K_2O	2.01	2.47	4.21	3.27	1.19	3.32	4.91	1.71	1.86	3.18	0.95
P_2O_5	0.05	0.20	NA	NA	0.02	NA	NA	NA	NA	0.05	0.24
LOI	1.49	1.19	NA	NA	1.28	NA	NA	NA	NA	1.47	0.90
Total	97.35	96.48	99.14	98.76	97.75	101.42	99.17	98.48	98.32	100.56	100.01

Site 2/2S

	F-2A/x	P-2A/bx	P-2A/br	P-2A/mr	B-2A/x	F-2S/x	P-2S/bx	P-2S/mr	IG-2S/x	B-2S/x
SiO_2	67.55	60.56	62.00	60.00	49.51	66.50	57.73	57.43	61.55	48.45
TiO_2	0.42	0.50	0.54	0.56	1.78	0.21	0.65	0.89	0.66	0.62
Al_2O_3	15.28	13.99	14.09	15.42	12.53	17.68	16.08	16.62	14.91	16.42
FeO*	2.38	6.09	6.70	7.19	16.79	1.63	6.48	7.18	5.44	7.76
MnO	0.05	0.11	0.06	0.06	0.30	0.03	0.08	0.05	0.05	0.13
MgO	1.84	4.71	4.37	4.81	4.63	1.31	4.94	5.89	3.55	9.99
CaO	3.62	5.40	5.88	6.14	8.50	2.45	4.69	3.57	3.44	11.34
Na_2O	4.61	2.25	2.51	2.56	1.31	4.73	3.22	2.76	3.34	1.86
K_2O	1.27	3.56	3.16	3.58	1.04	5.10	2.88	5.49	2.54	0.43
P_2O_5	0.12	0.10	NA	NA	0.20	0.24	NA	NA	0.16	0.05
LOI	0.79	1.36	NA	NA	0.79	NA	NA	NA	1.49	1.98
Total	97.93	98.63	99.31	100.32	99.26	99.88	96.75	99.88	97.75	99.90

Site 3

	F-3A/x	P-3A/br	P-3A/mr	F-3B/x	P-3B/br	P-3B/mr	B-3C/x
SiO_2	71.91	66.81	66.30	64.00	64.62	64.58	50.16
TiO_2	0.16	0.83	0.86	0.64	0.86	0.95	0.81
Al_2O_3	12.97	12.70	13.93	16.39	13.07	13.49	13.54
FeO*	1.19	6.42	6.25	1.79	7.68	7.14	10.42
MnO	0.02	0.03	0.06	0.05	0.05	0.05	0.20
MgO	0.49	2.74	2.76	0.75	3.22	2.91	8.37
CaO	2.09	1.50	1.49	2.91	1.34	1.50	11.01
Na_2O	3.28	4.84	5.74	5.97	4.55	5.04	0.30
K_2O	5.09	2.75	2.74	4.78	3.35	3.11	1.23
P_2O_5	0.04	NA	NA	0.19	NA	NA	0.07
LOI	0.60	NA	NA	0.84	NA	NA	2.74
Total	97.84	98.62	100.13	98.31	98.74	98.77	100.01

rocks (Fig. 4a). MgO shows a similar relationship, though there is some overlap with the felsic gneisses and granitoids at lower MgO values (Fig. 4b). Overall, there is an inverse relationship between SiO_2 and the ferromagnesian oxides (Fig. 4c), with SiO_2 + FeO* (total iron as FeO) + MgO + TiO_2 + MnO totalling 75 wt% oxides for all pseudotachylytes and host rocks. With the exception of the basic host rocks, there is a positive correlation between MgO and FeO*, with the mean MgO:FeO approximating 0.66 (Fig. 4d).

The most basic pseudotachylyte analyses were obtained from an injection vein (sample P-1B/i, Table 1; labelled α for matrix-only and β for bulk pseudotachylyte in Fig. 4a–d). This is an offshoot from a source horizon now occupied by pseudotachylyte P-1B (Table 1; labelled γ for matrix-only and δ for bulk in Fig. 4a–d). The pseudotachylyte occupying the source horizon clearly truncates the injection vein and so must post-date it. These four samples show a progressive increase in SiO_2 and a decrease in ferromagnesian oxides from α

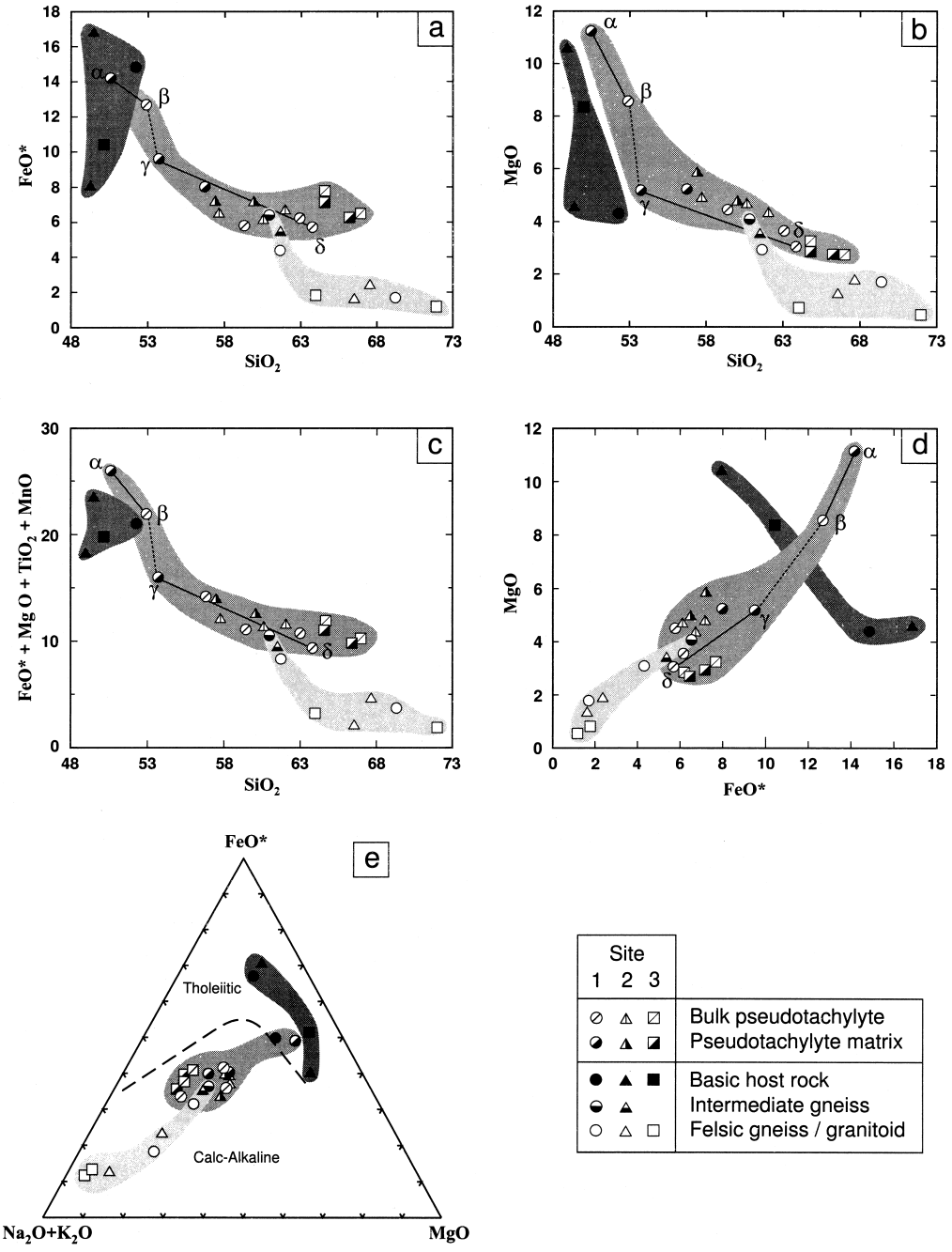

Fig. 4 Comparisons between: **a** FeO*; **b** MgO and **c** FeO* + MgO + TiO_2 + MnO and SiO_2; **d** MgO and FeO* and **e** alkalis - FeO* - MgO for host rock and bulk pseudotachylyte and pseudotachylyte matrix analyses in weight percent. Data from Table 1. α and β are the matrix-only and bulk compositions, respectively, of an injection pseudotachylyte. γ and δ are the matrix-only and bulk compositions, respectively, of a more evolved cross-cutting pseudotachylyte. FeO* is total iron in ferrous state

through to δ. For each pair, the matrix is more basic than its bulk composition – a feature common to most of the analysed pairs in this study (Table 1) and for pseudotachylytes in general (Reimold 1991; Spray 1993). Furthermore, the injection vein is more basic than the later pseudotachylyte. Significantly, this indicates that pseudotachylyte formation does not involve the bulk melting of host rocks, but rather selective melting with the initial product being more basic, as exemplified by the early injection vein, and subsequent melts being more silicic as they evolve towards a bulk composition. However, bulk melting appears to be rarely, if ever, achieved because the more felsic components, especially quartz, remain in the solid state as clasts.

Except for the injection vein (samples α and β, Table 1), the pseudotachylytes possess higher total alkali contents than the basic host rocks and plot in the calc-alkaline field (Fig. 4e). They also define an array that tends towards an andesitic composition. Along with the basic host rocks, the injection vein pair lie in the tholeiitic field.

There is an inverse relationship between the alkalis and CaO as indicated by Fig. 5a,b. This is illustrated by the behaviour of the injection vein and source horizon pseudotachylyte (Fig. 5). Unlike the alkalis, CaO behaves like the ferromagnesian oxides, showing an inverse relationship with SiO_2.

Overall, the compositions of the Sudbury pseudotachylytes lie between those of the acidic and basic host

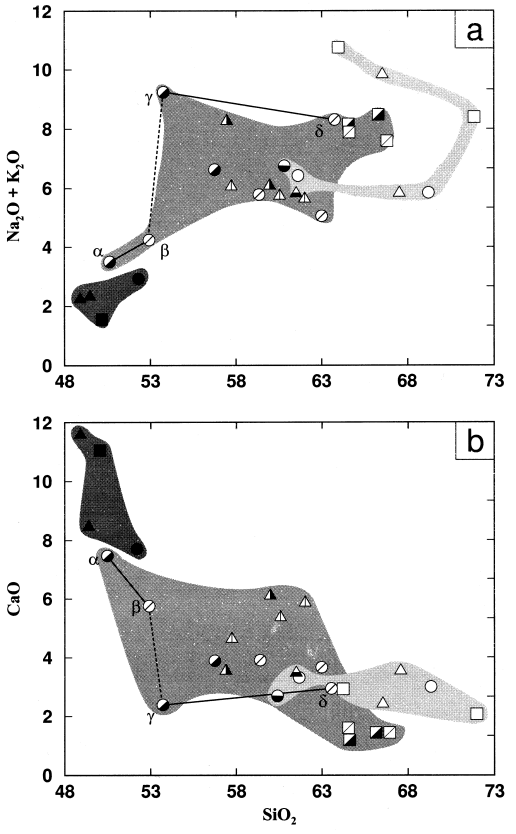

Fig. 5 **a** Sum of alkalis versus SiO_2 and **b** CaO versus SiO_2. Symbols as for Fig. 4

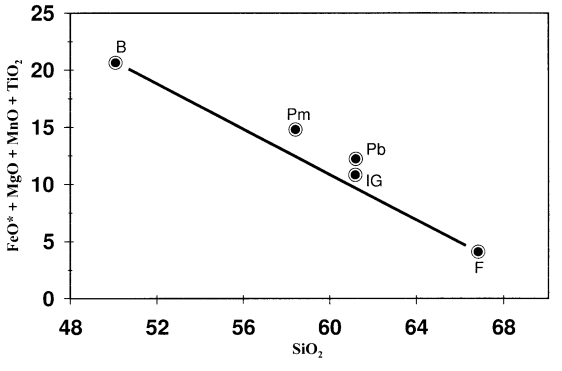

Fig. 6 Average compositions for all analysed pseudotachylytes and host rocks plotted as ferromagnesian oxides versus SiO_2 in weight percent. [*B* basic host rocks (n = 4), *IG* intermediate gneisses (n = 2), *F*: felsic gneisses and granitoids (n = 6), *Pm* pseudotachylyte matrices (n = 7), *Pb* bulk pseudotachylytes (n = 9)]

rocks, indicating that the pseudotachylytes are a blend of these end-members (Fig. 6). The bulk pseudotachylyte (matrix-plus-clast) compositions (denoted Pb), whether determined by XRF or by ASEM, lie between their respective acidic host rock and matrix-only compositions (denoted Pm), yet closer to the matrix-only values than the acidic hosts. Figure 6 suggests that the *average* bulk pseudotachylyte composition can be derived by the *in situ* comminution and partial melting of acidic (felsic gneisses plus granitoids) and basic host rocks in the proportions 60:40 respectively. Although the intermediate gneisses possess similar compositions to the pseudotachylytes, the relative scarcity of these gneisses at the studied sites suggests that their contribution to pseudotachylyte production was negligible.

Host rock mineralogy

Rocks of the Archean Levack gneiss complex are the main host to pseudotachylytes at Sites 1 and 2S and are a subordinate host at Site 2. These rocks are composed of coarse-grained quartz - plagioclase - potassium feldspar - biotite - calcic amphibole assemblages, retrogressed from the granulite facies (James et al. 1991). Plagioclase ranges from albite to andesine (An_{2-28}) (Table 2) and exhibits saussuritization and rare PDFs. Quartz is typically partly recrystallized, but otherwise shows undulose extinction, fracturing and decorated PDFs. Potassium feldspar occurs as microcline (Or_{98}) and as untwinned orthoclase with a cloudy, altered appearance (Table 3). Antiperthites are also observed with host plagioclase compositions of An_{25} and K-feldspar blebs of Or_{96}. Pleochroic deep brown biotite is the dominant mafic phase, showing kinking and inclusion trails of opaque oxides (Table 4, Fig. 8). Actinolitic hornblende is a minor constituent of the felsic gneisses at Site 1. Intermediate gneisses are more biotite rich.

The main hosts to the pseudotachylyte at Sites 2 and 3 are the Archean Cartier granitoids. These consist of quartz, potassium feldspar, plagioclase, biotite, chlorite and epidote. At Site 3 this assemblage is largely secondary, due to retrograde effects associated with the Benny deformation zone (Card 1994). Plagioclase is saussuritized (Table 2) and quartz is recrystallized, but locally exhibits decorated PDFs, undulose extinction and fracturing. Potassium feldspar occurs as orthoclase (Or_{100}) (Table 3) and within perthite. Unlike the Levack biotites, those from the Cartier granitoids are pleochroic green–brown and do not exhibit kinking (Table 4). Chlorite is observed intergrown with and replacing biotite.

Basic igneous intrusions occur at all three sites as part of regional dyke swarms. The gabbroic intrusion from Site 2S has a primary mineralogy of augite, orthopyroxene, olivine and plagioclase (An_{45}). The augite is partly replaced by hornblende and the plagioclase is saussuritized. All other basic intrusive rocks are more severely retrogressed. They contain magnesio- or pargasitic hornblende partly replaced by actinolite. In places, biotite replaces amphibole, titanite occurs after ilmenite and plagioclase (An_{44}) is saussuritized. Chlorite, epidote, clinozoisite, quartz and opaques are present in minor amounts.

Table 2 ASEM analyses of plagioclase from host rocks and pseudotachylytes. Formulae calculated on the basis of 8 oxygens. (*Wt%* weight percent, *Form* formula, *c* clast, *o* overgrowth, *y* crystal, *An* anorthite content of the plagioclase in%, *0.00* not detected)

Host rocks								
	F-1B Wt%	An11 Form	F-2A Wt%	An24 Form	F-2A Wt%	An6 Form	F-3 Wt%	An1 Form
SiO_2	64.92	2.89	62.65	2.77	67.16	2.96	69.73	3.00
TiO_2	0.00	0.00	0.00	0.00	0.00	0.00	0.00	0.00
Al_2O_3	21.07	1.11	23.43	1.22	20.17	1.05	19.78	1.00
FeO	0.00	0.00	0.00	0.00	0.19	0.01	0.00	0.00
MgO	0.00	0.00	0.00	0.00	0.00	0.00	0.00	0.00
CaO	2.36	0.11	5.15	0.24	1.26	0.06	0.20	0.01
Na_2O	9.22	0.80	8.75	0.75	10.26	0.88	10.44	0.88
K_2O	1.42	0.08	0.10	0.01	0.05	0.00	0.05	0.00
Total	98.99		100.08		99.09		100.20	

Pseudotachylytes								
	Clasts						Metamorphic	
	P-1A/c Wt%	An31 Form	P-2B/c1 Wt%	An28 Form	P-2B/c2 Wt%	An32 Form	P-3 Wt%	An5 Form
SiO_2	61.10	2.72	61.25	2.73	60.56	2.67	67.01	2.93
TiO_2	0.00	0.00	0.00	0.00	0.00	0.00	0.00	0.00
Al_2O_3	24.35	1.28	24.09	1.26	25.30	1.31	20.81	1.07
FeO	0.39	0.01	0.21	0.01	0.26	0.01	0.13	0.00
MgO	0.00	0.00	0.00	0.00	0.34	0.02	0.19	0.01
CaO	6.06	0.29	5.86	0.28	6.71	0.32	1.24	0.05
Na_2O	7.57	0.65	8.18	0.71	7.76	0.66	11.00	0.93
K_2O	0.14	0.01	0.12	0.01	0.12	0.01	0.07	0.00
Total	99.61		99.71		101.05		100.45	

	Neo-igneous							
	P-1A/o Wt%	An52 Form	P-2B/o1 Wt%	An56 Form	P-2B/o2 Wt%	An49 Form	P-2B/y Wt%	An63 Form
SiO_2	55.07	2.50	54.27	2.45	56.64	2.52	52.75	2.39
TiO_2	0.00	0.00	0.11	0.00	0.00	0.00	0.00	0.00
Al_2O_3	27.23	1.46	28.19	1.50	27.42	1.44	29.78	1.59
FeO	0.93	0.04	0.81	0.03	0.93	0.04	0.39	0.01
MgO	0.24	0.02	0.00	0.00	0.46	0.03	0.00	0.00
CaO	10.68	0.52	11.73	0.57	10.23	0.49	12.93	0.63
Na_2O	5.29	0.47	5.00	0.44	5.91	0.51	4.20	0.37
K_2O	0.21	0.01	0.11	0.01	0.00	0.00	0.06	0.00
Total	99.65		100.22		101.59		100.11	

Pseudotachylyte mineralogy

Three distinct assemblages are identified within the pseudotachylytes: (1) an inherited mineralogy, derived from the host rocks, as preserved in rock and mineral clasts; (2) a neo-igneous mineralogy, formed due to crystallization from a melt, as locally preserved in the matrices; (3) a post-impact retrograde mineralogy overprinting both clasts and matrices.

Inherited mineralogy

Lithic clasts, as well as monomineralic clasts derived from the Levack gneiss complex, Cartier granitoids and basic host rocks have been incorporated into the pseudotachylytes.

Quartz is the most abundant mineral clast, exhibiting features common to the host lithologies (e.g. remnant PDFs) as well as corroded and embayed contacts with the matrices. Quartz clasts in the pseudotachylytes from Site 3 are, however, recrystallized to a polygonized texture of unstrained subgrains.

Plagioclase clasts are also ubiquitous in the pseudotachylytes, with matrix contact relations similar to those of quartz (Fig. 7a). However, the clasts are typically

Table 3 ASEM analyses of K-feldspar from host rocks and pseudotachylytes. Formulae calculated on the basis of 8 oxygens. (*Or* orthoclase content of potassium feldspar in %, *0.00* not detected). *i* pseudotachylyte injection

Host rocks								
	F-1B Wt%	Or98 Form	F-2A Wt%	Or98 Form	F-2B Wt%	Or98 Form	F-3 Wt%	Or100 Form
SiO_2	68.91	3.13	64.75	3.00	68.91	2.96	64.01	3.00
TiO_2	0.11	0.00	0.00	0.00	0.11	0.00	0.19	0.01
Al_2O_3	15.75	0.84	18.03	0.98	15.75	0.84	18.14	1.00
FeO	0.15	0.01	0.00	0.00	0.15	0.01	0.00	0.00
MgO	0.00	0.00	0.00	0.00	0.00	0.00	0.00	0.00
CaO	0.00	0.00	0.00	0.00	0.00	0.00	0.00	0.00
Na_2O	0.21	0.02	0.23	0.02	0.21	0.02	0.00	0.00
K_2O	15.02	0.87	17.15	1.01	15.02	0.87	16.39	1.00
Total	100.15		100.16		100.15		98.73	

Pseudotachylytes								
	Neo-igneous							
	P-1A Wt%	Or100 Form	P-1B/i Wt%	Or86 Form	P-1B/i Wt%	Or95 Form	P-1B Wt%	Or75 Form
SiO_2	64.18	2.97	63.41	2.93	64.52	3.00	63.97	2.93
TiO_2	0.25	0.01	0.24	0.01	0.26	0.01	0.26	0.01
Al_2O_3	18.80	1.03	18.69	1.02	17.63	0.96	19.48	1.05
FeO	0.34	0.01	0.78	0.03	0.59	0.02	0.71	0.03
MgO	0.00	0.00	0.47	0.04	0.44	0.03	0.27	0.02
CaO	0.00	0.00	0.86	0.04	0.33	0.02	1.32	0.06
Na_2O	0.00	0.00	1.08	0.10	0.29	0.03	1.99	0.18
K_2O	16.47	0.97	14.67	0.87	16.02	0.95	12.09	0.71
Total	100.04		100.20		100.08		100.09	
	P-2A Wt%	Or96 Form	P-2A Wt%	Or76 Form	P-2B Wt%	Or94 Form	P-2B Wt%	Or60 Form
SiO_2	65.82	3.03	65.89	3.00	63.98	2.96	65.43	2.96
TiO_2	0.46	0.02	0.33	0.01	0.45	0.02	0.68	0.02
Al_2O_3	17.54	0.95	17.75	0.95	18.48	1.01	19.02	1.01
FeO	0.33	0.01	0.56	0.02	0.38	0.01	0.24	0.01
MgO	0.00	0.00	0.45	0.03	0.00	0.00	0.00	0.00
CaO	0.16	0.01	1.96	0.10	0.29	0.01	0.83	0.04
Na_2O	0.30	0.03	1.23	0.11	0.56	0.05	3.84	0.34
K_2O	15.60	0.92	11.59	0.67	16.06	0.95	10.05	0.58
Total	100.21		99.76		100.20		100.09	

streaked out and contorted. Alkali feldspar clasts are less common in the pseudotachylytes, but they too exhibit ductile textures. Both the plagioclase and alkali feldspar clast compositions are identical to those of their host rock minerals.

Neither monomineralic biotite nor amphibole clasts were observed within the pseudotachylytes, though both may occur preserved within the larger composite (lithic) clasts.

Laser-probe Ar-Ar dating (unpublished data), using a 50–100 μm diameter focused infrared laser beam, of selected pseudotachylyte clast components from Site 3 and sites further north, yielded late Archean to early Proterozoic ages of 2.7–2.2 Ga, compatible with previously published ages obtained from the basement rocks of the North Range (Krogh et al. 1984).

Neo-igneous mineralogy

This is typified by the cryptocrystalline and micro-igneous-textured matrix of pseudotachylyte P-2B, as well as by samples P-1A and P-2A. Sample P-2B consists of ~10 μm crystallites of biotite (phlogopitic) + plagioclase ($An_{45–64}$) + orthoclase ± sanidine (Fig. 7b). Minor interstitial (neo-crystalline) quartz is present, but is sparse compared to its abundance as a clast phase. Neocrystals of alkali feldspar have two distinct compositions: orthoclase/microcline (e.g. Or_{94}) and a Na-K mixed phase ($Or_{60–76}$) showing no evidence of exsolution at the SEM scale. It is therefore not perthite (100–1000 μm), microperthite (5–100 μm) or cryptoperthite (1–5 μm), but probably sanidine (Table 3). X-ray diffraction analysis of sample P-2B confirms the presence of

Table 4 ASEM and electron microprobe analyses of biotites from host rocks and pseudotachylytes. Formulae calculated on the basis of 22 oxygens.

Host rocks

	F-1A Wt%	Form	F-1B Wt%	Form	F-2 Wt%	Form	F-3 Wt%	Form
SiO_2	35.79	6.01	35.17	5.49	36.52	5.57	35.93	5.56
TiO_2	1.85	0.23	1.77	0.21	1.33	0.15	1.47	0.17
Al_2O_3	16.47	3.26	16.03	2.95	16.72	3.01	15.81	2.88
FeO	19.84	2.78	21.66	2.83	19.22	2.45	21.63	2.80
MnO	0.23	0.03	0.25	0.03	0.19	0.02	0.26	0.03
MgO	10.98	2.75	10.27	2.39	11.09	2.52	10.55	2.43
CaO	0.00	0.00	0.00	0.00	0.29	0.05	0.00	0.00
Na_2O	0.00	0.00	0.00	0.00	0.00	0.00	0.00	0.00
K_2O	9.82	2.10	9.26	1.84	10.12	1.97	9.53	1.88
Total	94.98		94.41		95.48		95.18	

Pseudotachylytes

	P-1A Wt%	Form	P-1B Wt%	Form	P-2B Wt%	Form	P-3 Wt%	Form
SiO_2	40.53	6.00	37.02	5.63	39.66	5.83	36.07	5.61
TiO_2	1.23	0.10	1.08	0.12	1.77	0.20	1.59	0.18
Al_2O_3	14.80	2.60	16.78	3.01	15.66	2.72	15.51	2.84
FeO	17.82	2.20	20.43	2.60	16.62	2.04	21.08	2.74
MnO	0.22	0.00	0.21	0.03	0.22	0.03	0.31	0.04
MgO	11.50	2.54	11.12	2.52	12.88	2.83	10.08	2.34
CaO	1.83	0.30	0.09	0.01	0.53	0.08	0.00	0.00
Na_2O	0.00	0.00	0.69	0.20	0.00	0.00	0.00	0.00
K_2O	8.09	1.50	7.23	1.40	9.30	1.74	10.01	1.99
Total	96.02		94.65		96.64		94.65	

sanidine. Significantly, alkali feldspar of this composition was not found in any of the analysed host rocks or clasts.

Biotite is abundant in the matrices. It occurs as needles and as irregular-shaped crystals intergrown with the feldspars (Fig. 7b). The biotites have an average composition distinct from that of their host rocks, tending to be more phlogopitic (Table 4, Fig. 8).

Plagioclase within the matrices occurs in BSE imagery as light grey laths (Fig. 7b) and overgrowths mantling a darker grey plagioclase (Fig. 7c). The darker grey centres have an average oligoclase composition (An_{23}), identical to that of host rock plagioclase (Table 2), and these are interpreted as clasts. The mantling plagioclase typically forms a uniform halo with sharp contacts around the oligoclase (Fig. 7c). Overgrowth compositions range from An_{45} to An_{56} with an average of An_{51} (labradorite) (Table 2). Certain plagioclase overgrowths are themselves zoned, with a slightly lighter grey (more An-rich) area closer to the centre and a darker grey (less An-rich) rim. Less commonly, the plagioclase overgrowths occur as radiating crystallites $\sim$5 μm long. Plagioclase neo-crystals in the matrices range from An_{52} to An_{64}, with an average of An_{57} (labradorite) (Table 2). Figure 9 shows the distinction between the compositions of the host rock clasts and those of the mantling labradorite and labradorite neo-crystals. The single clast with the anomalously high An content is from a rare gabbro inclusion. Occasional bytownite clasts, presumably also derived from basic host rocks, are also found with labradorite overgrowths.

Quartz + phlogopitic biotite + sanidine + labradorite is considered a high temperature assemblage that crystallized from a melt. The original existence of melt is supported by the embayed and corroded nature of the quartz and feldspar mineral clasts, as well as the presence of vesicles in sample P-1A. Müller-Mohr (1992, p. 222) describes rosette-like growths of pyroxene in his type 3C pseudotachylytes from the North Range, which also suggest a melt origin. Relatively rapid cooling of the melt is indicated by the presence of sanidine and by the microcrystalline grain sizes.

Laser-probe Ar-Ar dating of certain pseudotachylyte matrix phases sampled 65 km north of the SIC yielded ages of $\sim$1.85 Ga (Thompson et al. 1994), compatible with the timing of the impact event (Krogh et al. 1984). We attribute this result to the dating of neo-igneous K-bearing phases (i.e. biotite and K feldspar) within the pseudotachylyte matrix.

Post-impact retrograde mineralogy

Both host rocks and pseudotachylytes have undergone a number of tectonothermal events following impact (e.g. Penokean and, on a local scale in the North Range, even Grenvillian). These events have obscured, but not completely supplanted, pre-existing mineral assemblages.

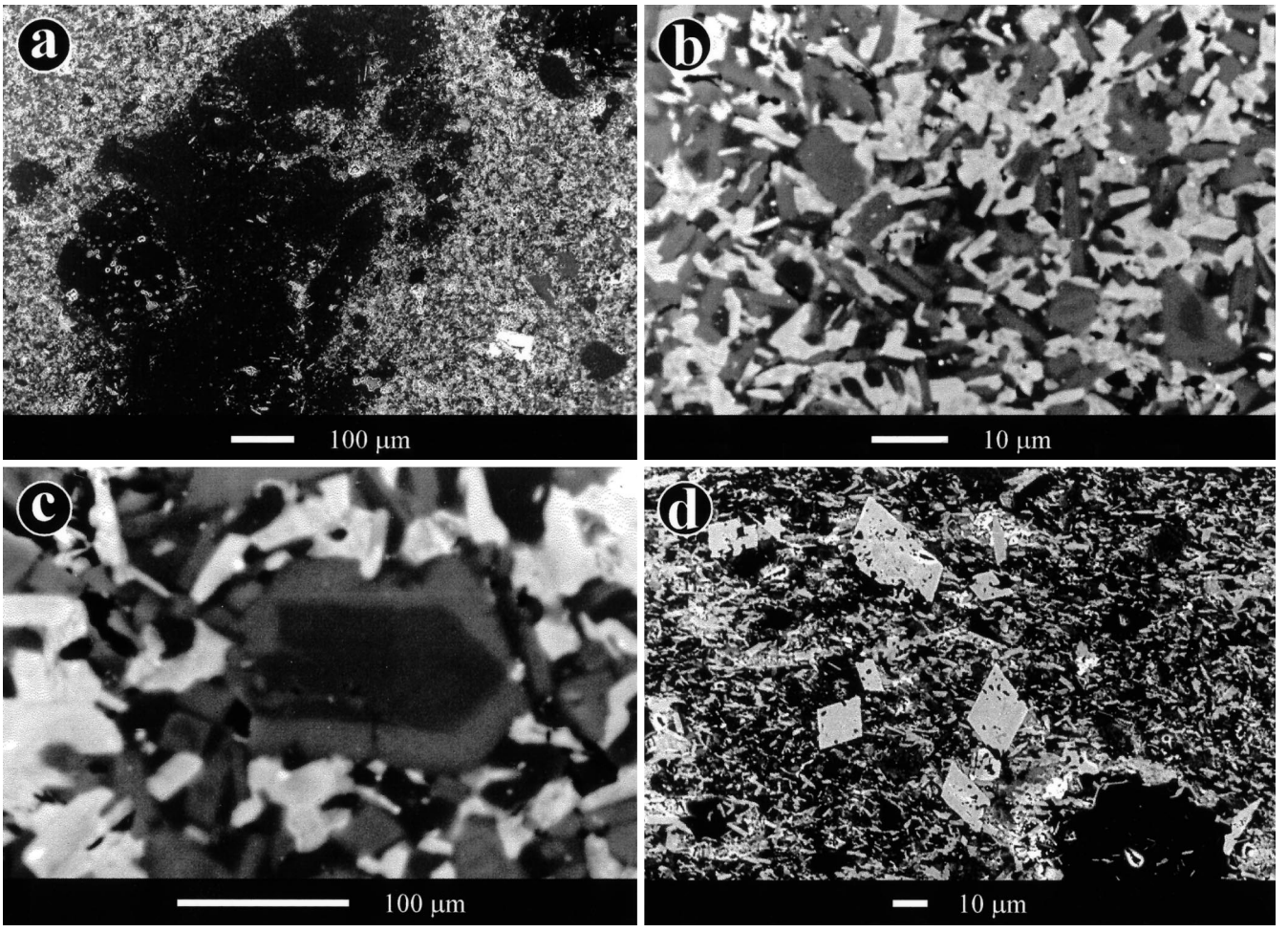

Fig. 7 SEM backscattered electron photomicrographs of: **a** plagioclase clast (*black*) from sample P-2B showing partial injection/assimilation by pseudotachylyte matrix. **b** Typical pseudotachylyte matrix (sample P-2B). Micro-igneous-textured phlogopitic biotite (*off white*), labradorite (*grey*) occurring as needle-like crystals and as overgrowths surrounding oligoclase/andesine clasts (*dark grey*), as in *bottom right hand corner*, and quartz (*black*). **c** Close-up of labradorite overgrowth (*light grey*) mantling an oligoclase clast (*dark grey*). Phlogopitic biotite (*lightest grey*) in matrix, is intergrown with the labradorite overgrowth. Note presence of labradorite crystals (*light grey*) and interstitial quartz (*black*) in the matrix. **d** Cryptocrystalline-textured matrix of pseudotachylyte P-2A, showing post-impact retrograde effects. Large epidote porphyroblasts (*lightest grey* rhombic crystals) overgrow both matrix components and clasts

The pseudotachylytes have been especially susceptible to alteration, probably because of their microcrystalline texture and due to fluid flow through host fault zones. Retrogression to greenschist and lower grade facies is common and, at least at Site 3, metamorphism was accompanied by metasomatism resulting in extensive epidote veining. Retrogression led to the development of secondary biotite, actinolite, albite, titanite, epidote, clinozoisite, chlorite and prehnite. The late biotites contrast with the biotite neo-crystals in having Fe>Mg, no interlayer Na or Ca and lower Si (Fig. 8; Table 4: F-3, P-3). Actinolite to actinolitic hornblende occurs in the

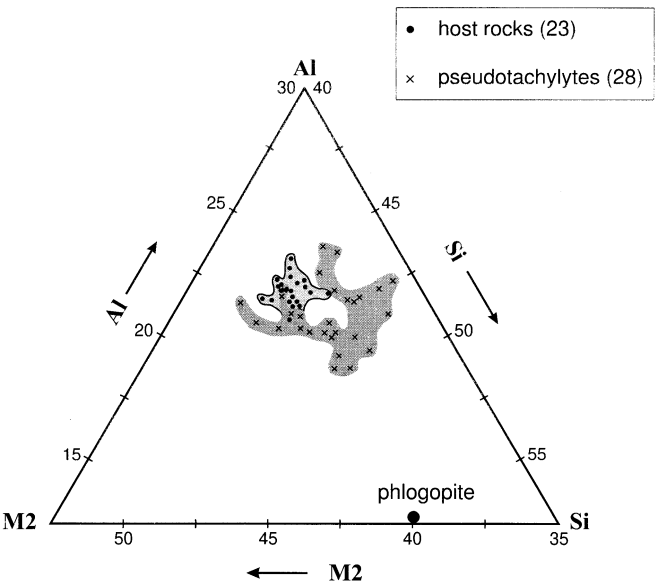

Fig. 8 Comparison of host rock and pseudotachylyte matrix biotite compositions. Primary biotites from pseudotachylyte matrices have higher Si and slightly lower M2 (M^{2+} cation) contents than host rock biotites. Pseudotachylyte matrix biotites with similar compositions to host rock biotites are considered to result from post-impact retrograde effects

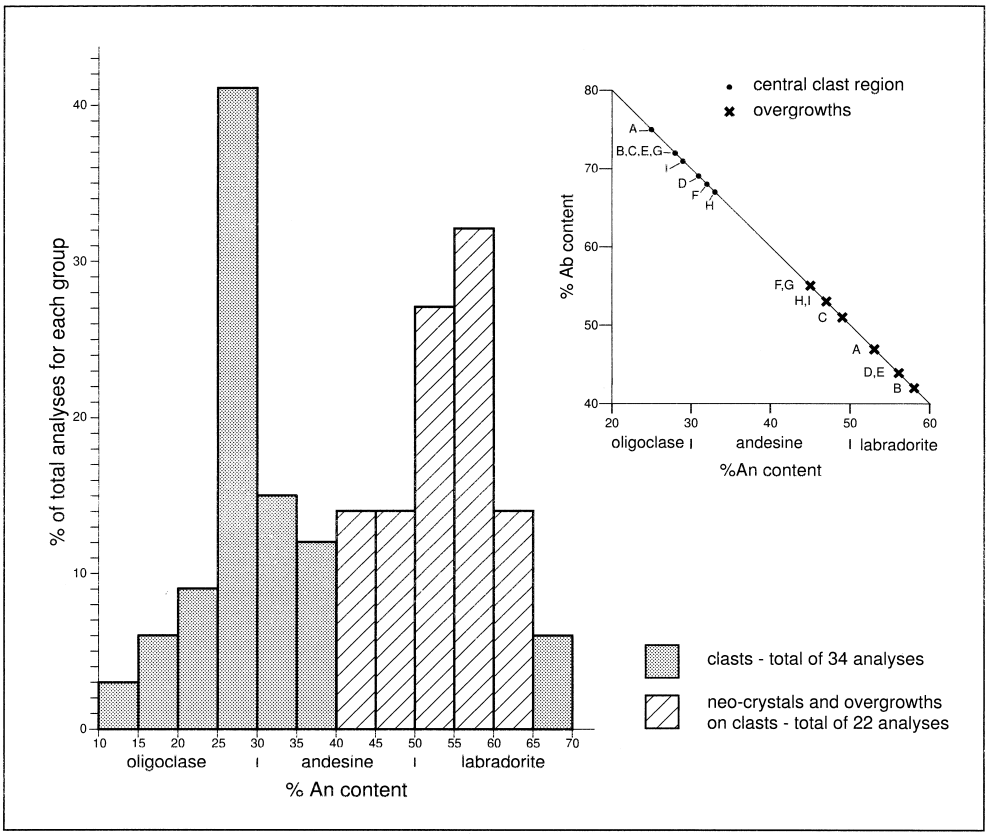

Fig. 9 Histogram of % total analyses for each range in composition (e.g. An_{20-25}) versus An content for sample P-2B plagioclases. This shows the distinction between plagioclase clasts whose compositions peak at An_{25-30} (oligoclase), and plagioclase neocrystals and overgrowths whose compositions peak at An_{55-60} (labradorite). The inset of %Ab versus %An contents shows the compositional relationships between clast-overgrowth pairs

Table 5. ASEM analyses of retrograde minerals in pseudotachylytes. Formulae calculated on the basis of 23 oxygens for amphibole, 12.5 for epidote, 28 for chlorite and 1 silica for titanite. (*0.00* not detected)

	Amphibole		Epidote		Chlorite		Titanite	
	P-1A Wt%	Form	P-2A Wt%	Form	P-3 Wt%	Form	P-2B Wt%	Form
SiO_2	53.06	7.69	37.90	2.97	25.76	5.64	31.01	1.00
TiO_2	0.22	0.02	0.00	0.00	0.00	0.00	34.81	0.86
Al_2O_3	2.57	0.44	24.46	2.26	19.05	4.92	2.57	0.09
FeO	13.19	1.60	9.84	0.64	25.67	4.70	2.10	0.04
MnO	0.48	0.06	0.18	0.01	0.49	0.09	0.00	0.00
MgO	14.89	3.22	0.00	0.00	13.91	4.54	1.22	0.06
CaO	12.42	1.93	23.79	2.00	0.00	0.00	24.99	0.86
Na_2O	0.48	0.14	0.00	0.00	0.00	0.00	0.00	0.00
K_2O	0.17	0.03	0.00	0.00	0.00	0.00	1.29	0.05
Total	97.48		96.17		84.88		97.99	

matrices of P-1A (Table 5), P-1B/i, P-2A and P-2B. Albite (An_5) is present in the pseudotachylyte matrices from Site 3 (Table 2). Epidote porphyroblasts, up to 100 μm across, overgrow both neo-crystals and clasts in sample P-2A (Table 5; Fig. 7d).

A laser-probe Ar-Ar age of ~1.57 Ga (unpublished data), indicative of the timing of a later, post-impact thermal event and/or movement on the Benny deformation zone, was obtained from an altered pseudotachylyte sample at Site 3.

Discussion

The Sudbury pseudotachylytes occur as thin veins and larger dyke-like bodies in the target rocks beneath the impact melt sheet (SIC) of the Sudbury structure. Their compositions, as determined by XRF and ASEM, indicate derivation from their host/wall rocks. Based on this study, the average pseudotachylyte can be produced by blending 60% felsic gneiss/granitoids with 40% basic host rocks. These melting proportions do not reflect the relative distribution of acidic versus basic rocks at the studied sites. This indicates that the basic host rocks were preferential sites for pseudotachylyte formation. Although the intermediate gneisses have similar compo-

sitions to some of the pseudotachylytes, they occur only in minor volumes, so their contribution to pseudotachylyte production is considered negligible. The preferential frictional melting of the more basic host rocks is in keeping with pseudotachylyte commonly being found developed along lithological contacts of marked ductility contrast (i.e. between felsic gneisses/granitoids and mafic dyke swarm material).

As with other documented pseudotachylyte occurrences (e.g. Maddock 1992; O'Hara 1992), the evidence presented here supports pseudotachylyte formation by the *in situ* comminution and frictional melting of fault walls during high-speed slip. A fault origin for the pseudotachylytes is supported by the association of the pseudotachylytes with discrete planar surfaces and, on the larger scale, with subconcentric zones developed about the SIC. The latter have been interpreted as the ring faults of a multi-ring impact basin (Spray and Thompson 1995). The formation of fault scarps as high as 6 km in lunar multi-ring impact basins indicates that such ring faults are capable of undergoing displacements of several kilometres in seconds/minutes during gravity-driven basin collapse (Melosh 1989). These displacements are substantially greater than the centimetre- to metre-scale offsets typical of endogenic faults. This explains how impact-generated pseudotachylytes can be several orders of magnitude larger than most of their endogenic counterparts. The amount of energy released during slip is the product of shear stress and displacement, so large-displacement faults are capable of releasing significantly more energy than are regular faults at a given shear stress. Energy is dissipated in the mechanical work exerted on the slip plane via comminution and heat production which leads to melting.

Establishing the degree of comminuted versus frictionally melted material present in a given pseudotachylyte is a difficult task, if not an intractable one when working in the field. Comminuted material/melt proportions depend on the prevailing strain rate and are best considered a continuum (Spray 1995). As such, the creation of an elaborate classification scheme for a continuum is unwarranted, except for distinguishing purely cataclastic rocks from those bearing some friction melt.

This work shows that the frictional melting process is unlike normal partial melting typical of adiabatic decompression. ASEM reveals that the pseudotachylytes comprise two distinct components: (1) inherited rock and mineral clasts, which are quartz- and plagioclase-rich, (2) matrices derived by comminution and melting of the host rocks. A given pseudotachylyte matrix is more basic than its bulk (matrix-plus-clast) composition. This shows that melting is selective such that host rock ferromagnesian phases are preferentially assimilated. The order of melting was hydrous ferromagnesian phases first (e.g. amphibole, biotite) followed by alkali feldspar, plagioclase and finally quartz. This is in accord with the sequence proposed by Spray (1992), where the frictional melting tendency of phyllosilicates > inosilicates (double chain > single chain) > tectosilicates (alkali feldspar > plagioclase > quartz) > orthosilicates. This sequence reflects the mechanical susceptibility of a mineral to comminution and eventual dissolution based on fracture toughness rather than indicating any form of equilibrium minimum melting process as would be expected for a normal melting scenario.

The proposed order of mineral melting is substantiated by the chemical evidence. The more basic composition of the injection vein P-1B/i, relative to the later truncating pseudotachylyte P-1B (Figs. 4a–e, 5a,b, Table 1) favours initial melting of an Fe, Mg and Ca-rich phase in the Levack gneiss host rocks (e.g. calcic amphibole) followed by a more alkali-rich phase (e.g. alkali feldspar) as comminution and melting proceed.

The development of labradorite overgrowths on oligoclase clasts, labradorite crystallites, sanidine crystallites and more phlogopitic biotite in the matrices indicate crystallization from a melt. According to the cotectic albite-anorthite-quartz-H_2O system at 200 MPa, An_{55} labradorite would crystallize from a melt at 780°C, and at 900°C at a P_{H2O} of 500 MPa (Deer et al. 1963). A temperature of 790°C was obtained from the isobaric equilibrium diagram for alkali feldspars at a P_{H2O} of 200 MPa, and 850°C at 500 MPa, for an Or_{70} (sanidine) composition (Johannes 1978, 1989). The crystallization temperature of the friction melt is therefore placed at 800–900°C. This must have been followed by relatively rapid cooling to prevent any observable exsolution of the Na-K feldspar at the SEM scale. Subsequent retrograde metamorphism has obliterated much of the neo-igneous mineralogy, such that preservation of high temperature assemblages is now sporadic.

Model for pseudotachylyte formation

The generation of pseudotachylyte within the Sudbury structure can be summarized as occurring in a number of stages as illustrated in Fig. 10.

1. Initial failure, fracturing and slip in discrete zones within the basement surrounding the transient cavity following meteorite impact at 1.85 Ga (Fig. 10a).
2. Comminution of material along slip surfaces resulting in a matrix of fine-grained, pulverized material with included angular fragments of the more resistant phases, i.e. quartz and feldspar (Fig. 10b).
3. The kinetic energy released during comminution results in heat generation which leads to fusion of the mechanically weakest (and, hence, finest) material first (i.e. hydrous ferromagnesian phases). This gives rise to a more mafic initial friction melt enclosing tougher clasts. Some of the smaller injection veins may become isolated from the main melt to preserve the initial more basic friction melt component (Fig. 10c).
4. As melt is continually generated along the slip plane, expansion due to melting leads to localized high pressure, explosive injection of melt into the wall rocks (Fig. 10d). This can lead to the formation of large volumes of brecciated wall rock embedded in pseudotachy-

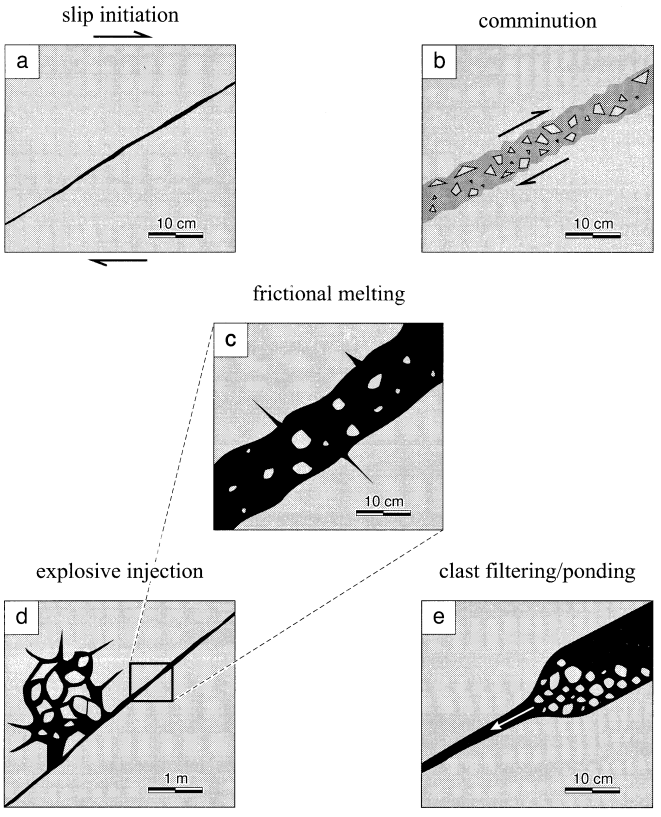

Fig. 10a–e Model for pseudotachylyte generation: **a** fracture and initiation of slip zone; **b** continued slip results in comminution of wall rocks – note angular clasts; **c** partial melting by friction, with the more mechanically resistant rock and mineral components surviving as clasts – note more rounded clasts; **d** explosive injection of pseudotachylyte from generating plane into wall rocks; displacement of clasts within injection can be negligible – note change of scale; **e** rock and mineral clasts may be filtered out, or may pond, to leave a matrix-rich, more basic pseudotachylyte

lyte matrix. In contrast to the more discrete generation planes, these areas, though conspicuous because of their size, may show little evidence of margin displacement or of rotation of enclosed rock clasts/blocks. The presence of large explosive injections provides an explanation for the observation that some of the larger Sudbury pseudotachylyte bodies show no evidence of displacement (e.g. Fairbairn and Robson 1942; Speers 1957).

5. Injection between slip planes continues eventually to form large pockets and dyke-like bodies. The melt partially assimilates the wall rocks and included clasts to evolve towards a bulk protolith composition. Clasts become rounded via abrasive wear, thermal fragmentation and assimilation. Clasts may also become "filtered" out or ponded leading to the creation of more basic, matrix-dominated zones "downstream" and less basic clast-rich zones "upstream" (Fig. 10e).

The above scenario is based on observations made at Sudbury, but may apply to other pseudotachylyte occurrences developed within both endogenic fault systems and impact structures. In this respect, we see no fundamental difference in the mechanism of pseudotachylyte formation (cf. Reimold 1995). With the possible exception of *Type A* pseudotachylytes, which may directly be shock generated, pseudotachylyte is formed by the frictionally induced comminution and partial melting of wall rocks during high-speed (seismogenic) slip. For the larger impact structures, this occurs during gravitational collapse of the transient cavity and, at least for the *Type B* pseudotachylytes, this post-dates the passage of the main shock front.

Acknowledgements This work forms part of L.M.T.'s PhD thesis and was funded by NSERC, EMR and LITHOPROBE grants to J.G.S.. We also acknowledge valuable support from the Ontario Geological Survey and INCO. Analytical electron microscopy and microprobe analysis were performed at UNB's Electron Microscopy Unit. Richard Kellett procured the core samples as part of a tandem magnetic study carried out during tenure of a two-year NSERC International Post-Doctoral Fellowship held with J.G.S. at UNB. Angel Gomez is thanked for help with drafting. Amy Prebble, Alastair Still and Susan Tingley assisted in the field during the summers of 1993 and 1994. We are grateful to Alex Deutsch and Uwe Reimold for constructively reviewing an earlier version of the manuscript.

References

Abbey S (1983) Studies in "standard samples" of silicate rocks and minerals: 1969–1982. Geol Surv Can Pap 83–15

Card KD (1994) Geology of the Levack gneiss complex, the northern footwall of the Sudbury structure, Ontario. In: Current research 1994-C. Geol Surv Can, pp 269–278

Card KD, Innes DG (1981) Geology of the Benny area, District of Sudbury. Ont Geol Surv Rep 206

Corfu F, Andrews A (1986) A U-Pb age for mineralized Nipissing diabase, Gowganda, Ontario. Can J Earth Sci 23: 107–112

Deer WA, Howie RA, Zussman J (1963) Framework silicates. (Rock-forming minerals, vol 4) Longmans, London

Deutsch A (1994) Isotope systematics support the impact origin of the Sudbury structure (Ontario, Canada). In: Dressler BO, Grieve RAF, Sharpton VL (eds) Large meteorite impacts and planetary evolution. Geol Soc Am, Boulder, Colorado, Spec Publ 293 pp 289–302

Deutsch A, Grieve RAF, Avermann M, Bischoff L, Brockmeyer P, Buhl D, Lakomy R, Müller-Mohr V, Ostermann M, Stöffler D (1995) The Sudbury structure (Ontario, Canada): a tectonically deformed multi-ring impact basin. Geol Rundsch 84: 697–709

Dietz RS (1964) Sudbury as an astrobleme. J Geol 72: 412–434

Dressler BO (1984) The effects of the Sudbury event and the intrusion of the Sudbury igneous complex on the footwall rocks of the Sudbury structure. In: Pye EG, Naldrett AJ, Giblin PE (eds) The geology and ore deposits of the Sudbury structure. Ont Geol Surv Spec Vol 1, pp 97–136

Faggart BE, Basu AR, Tatsumoto M (1985) Origin of the Sudbury complex by meteorite impact, neodymium isotopic evidence. Science 230: 436–439

Fairbairn HW, Robson GM (1942) Breccia at Sudbury, Ontario. J Geol 50: 1–33

French BE (1968) Sudbury structure, Ontario: some petrographic evidence for an origin by meteorite impact. In: French BM, Short NM (eds) Shock metamorphism of natural materials. Mono Book Corporation, Baltimore, pp 383–412

Grieve RAF, Stöffler D, Deutsch A (1991) The Sudbury structure: controversial or misunderstood? J Geophys Res 96: 22753–22764

Heaman LM (1988) A precise U-Pb age for a Hearst dike (abtract). Geol Assoc Can Mineral Assoc Can Program Abstr 13: A53

Hörz F (1968) Statistical measurements of deformation structures and refractive indices in experimentally shock loaded quartz.

In: French BM, Short NM (eds) Shock metamorphism of natural materials. Mono Book Corporation, Baltimore, pp 243–253

Hurst RW, Farhat J (1977) Geochronologic investigations of the Sudbury nickel irruptive and the Superior Province granites north of Sudbury. Geochim Cosmochim Acta 41: 1803–1815

James RS, Sweeny JM, Peredery WV (1991) Thermobarometry of the Levack gneisses – footwall rocks to the Sudbury igneous complex. Lithoprobe Abitibi–Grenville Transect Rep 32: 179–182

Jamieson RA, Culshaw NG, Wodicka N, Corrigan D (1992) Timing and tectonic setting of Grenvillian metamorphism – constraints from a transect along Georgian Bay, Ontario. J Metamorphic Geol 10: 321–332

Johannes W (1978) Melting of plagioclase in the system Ab-An-H_2O and Qz-Ab-An-H_2O at P_{H2O} = 5 kbar, an equilibrium problem. Contrib Mineral Petrol 66: 295–303

Johannes W (1989) Melting of plagioclase-quartz assemblages at 2 kbar water pressure. Contrib Mineral Petrol 103: 270–276

Joreau P, French BM, Doukhan J-C (1996) A TEM investigation of shock metamorphism in quartz from the Sudbury impact structure (Canada). Earth Planet Sci Lett 138: 137–143

Kennedy LA, Spray JG (1992) Frictional melting of sedimentary rock during high-speed diamond drilling: an analytical SEM and TEM investigation. Tectonophysics 204: 323–337

Killick AM (1990) Pseudotachylite generated as a result of drilling "burn-in". Tectonophysics 171: 221–227

Killick AM (1994) The geochemistry of pseudotachylite and its host rocks from the West Rand Goldfield, Witwatersrand Basin, South Africa: implications for pseudotachylyte genesis. Lithos 32: 193–205

Krogh TE, Davis DW, Corfu F (1984) Precise U-Pb zircon and baddeleyite ages for the Sudbury area. In: Pye EG, Naldrett AJ, Giblin PE (eds) The geology and ore deposits of the Sudbury structure. Ont Geol Surv Spec Vol 1, pp 431–448

Lakomy R (1990) Implications for cratering mechanics from a study of the Footwall Breccia of the Sudbury impact structure, Canada. Meteoritics 25: 195–207

Lambert P (1981) Breccia dikes: geological constraints on the formation of complex craters. Proc Lunar Planet Sci Conf 12A:59–78

Maddock RH (1983) Melt origin of fault-generated pseudotachylytes demonstrated by textures. Geology 11: 105–108

Maddock RH (1992) Effects of lithology, cataclasis and melting on the composition of fault-generated pseudotachylytes. Tectonophysics 204: 261–278

Magloughlin JF, Spray JG (1992) Frictional melting processes and products in geological materials: introduction and discussion. Tectonophysics 204: 197–206

Martini JEJ (1991) The nature, distribution and genesis of the coesite and stishovite associated with pseudotachylite of the Vredefort Dome, South Africa. Earth Planet Sci Lett 103: 285–300

Melosh HJ (1989) Impact cratering: a geologic process. Oxford University Press, New York

Müller-Mohr V (1992) Breccias in the basement of a deeply eroded impact structure. Tectonophysics 216: 219–226

Naldrett AJ (1984) Summary, discussion and synthesis. In: Pye EG, Naldrett AJ, Giblin PE (eds) The geology and ore deposits of the Sudbury structure. Ont Geol Surv Spec Vol 1: 533–569

Norrish K, Hutton JT (1969) An accurate X-ray spectrographic method for the analysis of a wide range of geological samples. Geochim Cosmochim Acta 33: 431–453

O'Hara K (1992) Major- and trace-element constraints on the petrogenesis of a fault-generated pseudotachylyte, western Blue Ridge province, North Carolina. Tectonophysics 204: 279–288

Ostertag R (1983) Shock experiments on feldspar crystals. J Geophys Res 88:B364–376

Peredery WV (1972) Chemistry of fluidal glasses and melt bodies in the Onaping Formation. In: Guy-Bray JV (ed) New developments in Sudbury geology. Geol Assoc Can Spec Pap 10, pp 49–59

Peredery WV, Morrison GG (1984) Discussion of the origin of the Sudbury structure. In: Pye EG, Naldrett AJ, Giblin PE (eds) The geology and ore deposits of the Sudbury structure. Ont Geol Surv Spec Vol 1, pp 491–511

Philpotts AR (1964) Origin of pseudotachylites. Am J Sci 262: 1008–1035

Reimold WU (1991) The geochemistry of pseudotachylites from the Vredefort Dome, South Africa. Neues Jahrb Mineral Abh 162: 151–184

Reimold WU (1995) Pseudotachylite in impact structures – generation by friction melting and shock brecciation?: a review and discussion. Earth-Sci Rev 39: 247–265

Rousell DH (1984) The Onwatin and Chelmsford Formations. In: Pye EG, Naldrett AJ, Giblin PE (eds) The geology and ore deposits of the Sudbury structure. Ont Geol Surv Spec Vol 1, pp 211–218

Schwarzman EC, Meyer CE, Wilshire HG (1983) Pseudotachylite from the Vredefort Ring, South Africa and the origins of Lunar breccias. Geol Soc Am Bull 94: 926–935

Shand SJ (1916) The pseudotachylyte of Parijs (Orange Free State) and its relation to "trapschotten gneiss" and "flinty crush rock". Q J Geol Soc London 72: 198–217

Shanks WS, Schwerdtner WM (1991) Structural analysis of the central and southwestern Sudbury structure, Southern Province, Canadian Shield. Can J Earth Sci 28: 411–430

Sibson RH (1975) Generation of pseudotachylyte by ancient seismic faulting. Geophys J R Astron Soc 43: 775–794

Speers EC (1957) The age relation and origin of common Sudbury Breccia. J Geol 65: 497–514

Spray JG (1987) Artificial generation of pseudotachylyte using friction welding apparatus: simulation of melting on a fault plane. J Struct Geol 9: 49–60

Spray JG (1988) Generation and crystallization of an amphibolite shear melt: an investigation using radial friction welding apparatus. Contrib Mineral Petrol 99: 464–475

Spray JG (1992) A physical basis for the frictional melting of some rock-forming minerals. Tectonophysics 204: 205–221

Spray JG (1993) Viscosity determinations of some frictionally generated silicate melts: implications for fault zone rheology at high strain rates. J Geophys Res 98: 8053–8068

Spray JG (1995) Pseudotachylyte controversy: fact or friction? Geology 23: 1119–1122

Spray JG, Rae DA (1995) Quantitative electron-microprobe analysis of alkali silicate glasses: a review and user guide. Can Mineral 33: 323–332

Spray JG, Thompson LM (1995) Friction melt distribution in a multi-ring impact basin. Nature 373: 130–132

Stöffler D, Langenhorst F (1994) Shock metamorphism of quartz in nature and experiment I. Basic observation and theory. Meteoritics 29: 115–181

Stöffler D, Deutsch A, Avermann M, Bischoff L, Brockmeyer P, Buhl D, Lakomy R, Müller-Mohr V (1994) The formation of the Sudbury structure, Canada: toward a unified impact model. In: Dressler BO, Grieve RAF, Sharpton VL (eds) Large meteorite impacts and planetary evolution. Geol Soc Am, Boulder, Colorado, Spec Publ 293, pp 303–318

Therriault AM, Reid AM, Reimold WU (1993) Original size of the Vredefort structure, South Africa. Lunar Planet Sci 24: 1419–1420

Thompson LM, Spray JG (1994) Pseudotachylytic rock distribution and genesis within the Sudbury impact structure. In: Dressler BO, Grieve RAF, Sharpton VL (eds) Large meteorite impacts and planetary evolution. Geol Soc Am, Boulder, Colorado, Spec Publ 293, pp 275–287

Thompson LM, Spray JG, Kelley SP (1994) Dating of pseudotachylytic rocks from the Sudbury impact structure via the laser probe ^{40}Ar-^{39}Ar technique: evidence for a 1.85 Ga formation event and post-impact thermal overprinting (abstract). Geol Soc Am Abstr Program 26:A425

Yates AB (1938) The Sudbury intrusive. Trans R Soc Can 32: 151–172

Zurbrigg HF (1957) The Frood-Stobie Mine. Can Inst Min Metall 2: 341–350